Chapter 1

Introduction

The present thesis explores two applications of two-dimensional correlation analysis: 1) detection of explosive compounds in the presence of dynamic background signals, and 2) categorizing and understanding transient structure development in semi-crystalline materials. Two-dimensional (2D) correlation analysis is a powerful technique that can be used to both visualize the relationship between intensity changes at different spectral points as a result of a perturbation and also elucidate the underlying physical phenomena causing the spectral response. It is applied to a set of one-dimensional (1D) data representing the response of a sample to a specific perturbation. Many scientific experiments result in these types of datasets, yet application of 2D correlation analysis is still mostly limited to the fields of optical and NMR spectroscopy, and furthermore applied predominately in a laboratory setting.

1.1 TWO-DIMENSIONAL CORRELATION SPECTROSCOPY

With roots in the field of nuclear magnetic resonance (NMR), two-dimensional (2D) correlation analysis (usually termed 2D correlation spectroscopy because of its frequent use in vibrational spectroscopy) allows one to examine the relationship between changes in spectral intensity at two different spectral variables in response to an external perturbation. Its application to vibrational spectroscopy was introduced by Isao Noda through the study of infrared (IR) spectral response to a sinusoidal perturbation,[1-3] and subsequently generalized to allow the use of a perturbation with arbitrary fluctuations.[4] Furthermore, in 2000, Noda introduced mathematical formulations based on the Hilbert-Noda transformation matrix that greatly simplified the analysis, allowing rapid processing of discrete datasets. These developments resulted in a significant increase in the popularity of 2D correlation spectroscopy.[5, 6]

Generalized two-dimensional correlation spectroscopy is based on the quantitative examination of spectral intensity changes as a function of the external perturbation, t, observed at two different spectral variables, v_1 and v_2 (for example, Raman shift as examined in Chapter 2 and scattering vector as examined in Chapter 4). Most commonly, analysis is conducted on a dynamic spectrum, which is defined for each value of the perturbation variable on its interval between T_{min} and T_{max} with respect to some reference spectrum, y_{ref}:

$$\widetilde{y}(v,t) = \begin{cases} y(v,t) - y_{ref}(v) & \text{for } T_{min} \leq t \leq T_{max} \\ 0 & \text{otherwise} \end{cases}. \tag{1.1}$$

A diversity of perturbation variables have been examined in literature, including strain, temperature, applied electric/magnetic field, irradiation, and time (see review by Noda[6]). The intensity at distinct spectral variables v_1 and v_2 tend to vary synchronously when they originate from the same molecular species or underlying physical process. Therefore, analysis of the synchronous two-dimensional correlation is a useful tool for identifying spectral changes that are intimately related. The intensity changes at distinct spectral variables tend to lag (lead) one another when, for example, formation of a given species is a prerequisite for a subsequent reaction to occur. Therefore, it is useful to characterize asynchronous two-dimensional correlations to identify spectral changes that occur sequentially.

The analysis may be readily understood for the simple case of a sinusoidal perturbation in the regime of linear response. A perturbation of the form $t = \text{Re}\{T'e^{i\omega\vartheta}\}$ having amplitude T' would elicit a response at each v_i that would oscillate at the same frequency, ω:

$$\widetilde{y}(v_i,t) = \mathrm{Re}\left\{A(v_i)e^{i(\omega\vartheta+\beta(v_i))}\right\} = \mathrm{Re}\left\{\hat{A}(v_i)e^{i\omega\vartheta}\right\}, \tag{1.2}$$

with amplitude $A(v_i)$ and phase $\beta(v_i)$. For distinct values of the spectral variable v_1 and v_2, the extent to which variation of intensity occurs simultaneously is captured by the "cospectrum,"

$$\phi_\omega(v_1,v_2) \equiv \mathrm{Re}\left\{\hat{A}(v_1)\cdot\hat{A}^*(v_2)\right\}, \tag{1.3}$$

and the extent which their variations lag (lead) one another is captured by the "quadspectrum,"

$$\psi_\omega(v_1,v_2) \equiv \mathrm{Im}\left\{\hat{A}(v_1)\cdot\hat{A}^*(v_2)\right\}, \tag{1.4}$$

where $\hat{A}^*(v_i)$ is the complex conjugate of $\hat{A}(v_i)$.

For a more complicated perturbation and spectral response composed of multiple sinusoids, the synchronous 2D correlation spectrum, $\Phi(v_1,v_2)$, is defined in terms of the cospectra as

$$\Phi(v_1,v_2) = \frac{1}{\pi}\int_0^\infty \phi_\omega(v_1,v_2)d\omega, \tag{1.5}$$

and the asynchronous 2D correlation spectrum, $\Psi(v_1,v_2)$, is defined in terms of the quadspectra as

$$\Psi(v_1,v_2) = \frac{1}{\pi}\int_0^\infty \psi_\omega(v_1,v_2)d\omega. \tag{1.6}$$

Noda further generalized this analysis to arbitrary functional forms of the perturbation, t, and spectral response, $\widetilde{y}(v_1,t) \equiv \widetilde{y}_1(t)$, by first decomposing the signal into sinusoids and representing it in the frequency domain with the application of the Fourier transform with respect to the perturbation, t:

$$\widetilde{Y}(v_1,\omega) = \int_{-\infty}^{\infty} \widetilde{y}(v_1,t)e^{-i\omega t}dt \,. \tag{1.7}$$

In this case of an arbitrary perturbation defined on the interval between T_{min} and T_{max}, the 2D correlation spectrum is given by

$$\Phi(v_1,v_2) + i\Psi(v_1,v_2) = \frac{1}{\pi(T_{max} - T_{min})} \int_{0}^{\infty} \widetilde{Y}_1(\omega) \cdot \widetilde{Y}_2^*(\omega)d\omega \,. \tag{1.8}$$

To circumvent the complexity and required computing power for the Fourier transform calculations, Noda used the well-known Wiener-Khintchine theorem to derive the 2D synchronous spectrum from the cross-correlation function[4,7] such that

$$\Phi(v_1,v_2) = \frac{1}{T_{max} - T_{min}} \int_{T_{min}}^{T_{max}} \widetilde{y}(v_1,t) \cdot \widetilde{y}(v_2,t)dt \,. \tag{1.9}$$

For a rigorous mathematical development, see Appendix 2.1 of reference [5].

The asynchronous spectrum can be computed from the cross-correlation of the dynamic spectrum, $\widetilde{y}(v,t)$, and its orthogonal spectrum, $\widetilde{z}(v,t)$:

$$\Psi(v_1,v_2) = \frac{1}{T_{max} - T_{min}} \int_{T_{min}}^{T_{max}} \widetilde{y}(v_1,t) \cdot \widetilde{z}(v_2,t)dt \,. \tag{1.10}$$

To calculate the orthogonal spectrum, Noda utilized the Hilbert transform, which has the effect of applying a phase shift of $\pi/2$ to each Fourier component of the dynamic spectrum, such that

$$\widetilde{z}(v,t) \equiv \frac{1}{\pi} \int_{Pv -\infty}^{\infty} \frac{\widetilde{y}(v,t)}{t'-t} dt' \,, \tag{1.11}$$

where $\int_{Pv}$ represents the implementation of the Cauchy principal value such that the singularity at $t = t'$ is excluded from the integration. Hilbert transform pairs, here $\widetilde{y}(v,t)$

and $\tilde{z}(v,t)$, are orthogonal. Hence, through the application of a phase shift in Fourier space, the asynchronous spectrum allows for the examination of temporal separation between intensity changes in real space.

To examine some of the advantages of 2D correlation analysis, let us consider a simulated dataset, $I(v,t)$ for $T_{min} \le t \le T_{max}$, containing three peaks (Figure 1.1a). The first peak increases quadratically in response to the perturbation, the second peak remains unchanged, and the third peak decreases linearly in the perturbation variable (Figure 1.1b).
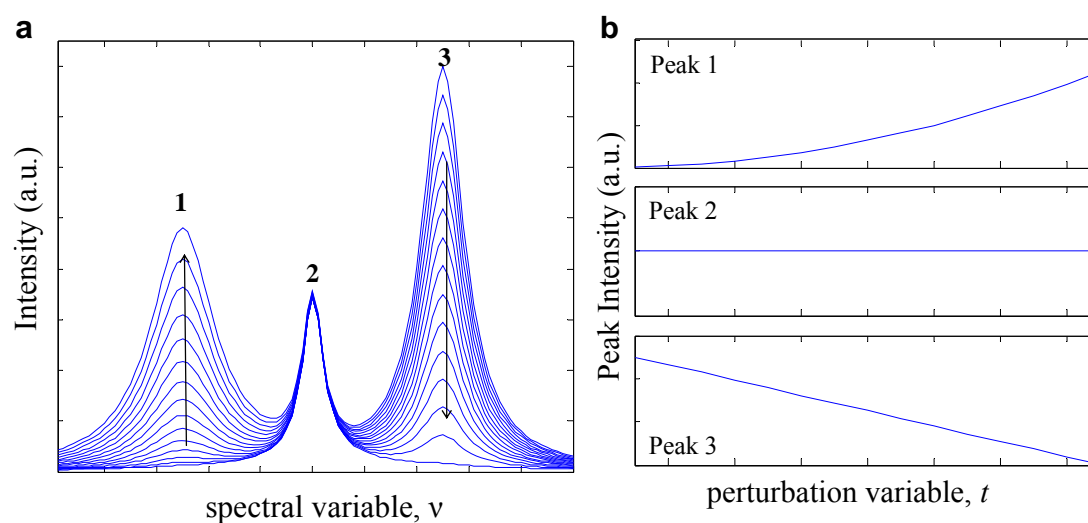
Figure 1.1 a) Simulated dataset. **b)** Evolution of peak intensities with perturbation of peaks in **a**.

The synchronous spectrum, $\Phi(v_1, v_2)$, is symmetric with respect to the diagonal ($v_1 = v_2$) and reveals simultaneous or coincident changes at two different spectral variables as the result of the perturbation. Consequently, in Figure 1.2, one observes two autopeaks along the diagonal corresponding to the intensity changes of peaks 1 and 3. The autocorrelation intensity along the diagonal is always positive and represents the total amplitude of the intensity variation in response to the perturbation.

In the off-diagonal position corresponding to peaks 1 and 3, one observes cross peaks indicating that the change in these two peaks occurs simultaneously. The negative sign of these features is consistent with the increase of peak 1 and a simultaneous decrease in peak 3 in response to the perturbation. The cross peaks are positive when intensity changes occur in the same direction.

The synchronous plot contains no features corresponding to peak 2 since there is no change in its intensity in response to the perturbation. This aspect of the 2D correlation analysis allows one to filter out static features, making it suitable for selective detection of compounds, as is discussed in Chapter 2.
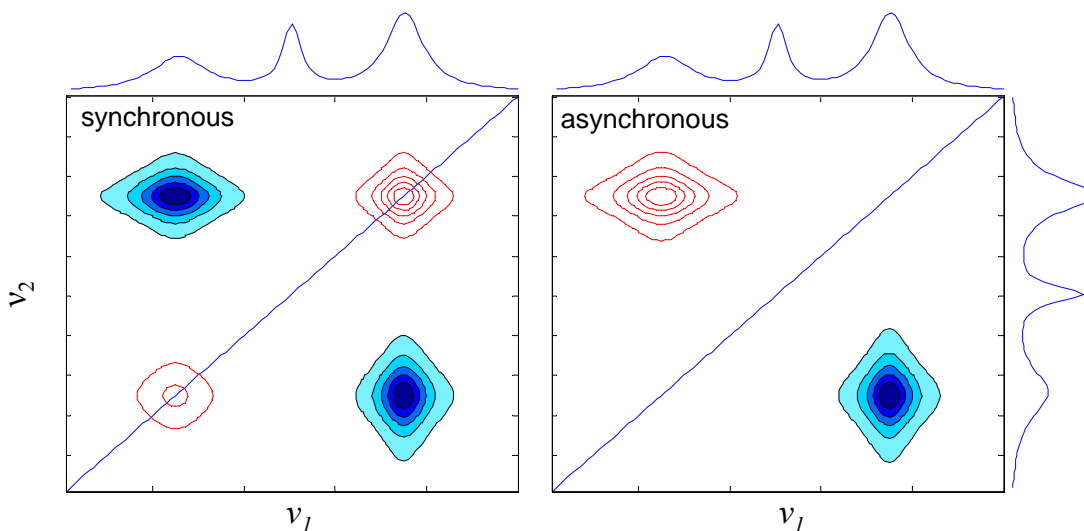
Figure 1.2 Synchronous (left) and asynchronous (right) spectra corresponding to simulated dataset in Figure 1.1. Shaded-in contours are negative, while non-shaded contours are positive. The average 1D spectra are plotted on the sides.

The 2D asynchronous spectrum, $\Psi(v_1, v_2)$, reveals the extent to which intensity changes at two spectral variables lead or lag one another during a perturbation. By its nature, it is antisymmetric and contains no autopeaks. In Figure 1.2, one observes features corresponding to peaks 1 and 3, indicating that there is temporal separation between these intensity changes.

The sign of the cross peaks reveals the sequential order of peak variations based on Noda's rules.[3, 5] Since the 2D asynchronous spectrum is anti-symmetric, it suffices to consider the region where $v_1 > v_2$ (below the diagonal). Interpretation of the sign of a cross peak at (v_1, v_2) when $v_1 > v_2$ in the asynchronous spectrum, $\Psi(v_1, v_2)$, depends on the sign of the intensity of the synchronous spectrum at (v_1, v_2): if $\Phi(v_1, v_2)$ is positive, then a positive asynchronous cross peak below the diagonal indicates that the response at v_1 precedes that at v_2; if $\Phi(v_1, v_2)$ is negative, then that positive cross peak indicates that the response at v_1 lags that at v_2 (Table 1.1). In the present case, negative features corresponding to peaks 1 and 3 are observed both in the synchronous and asynchronous plots. Therefore, the change in peak 3 precedes that in peak 1. This temporal separation can be interpreted in a more practical manner as a difference in half intensity and half time of peak evolution.[8] From Figure 1.1b, it is apparent that peak 3 has greater intensity half-way through the perturbation (half intensity) and achieves half of the total intensity change earlier along the perturbation (half time) than peak 1, resulting in changes in peak 3 preceding those in peak 1.

Table 1.1 Noda's Rules for sequential order when $v_1 > v_2$.

$\Phi(v_1, v_2)$	$\Psi(v_1, v_2)$	Interpretation
+	+	v_1 precedes v_2
+	−	v_1 lags v_2
−	+	v_1 lags v_2
−	−	v_1 precedes v_2

In reality, the analysis of 2D spectra can be quite complex, especially in the case of the asynchronous spectrum. The introduction of noise can often lead to artificial peaks in the asynchronous spectrum.[9, 10] Additionally, variations in the peaks themselves (i.e., position, shape, height, and width) can lead to patterns with multiple interpretations.[11-13]

These peak effects have been studied through simulated spectra revealing patterns in both the synchronous and asynchronous spectra that correspond to some commonly observed behaviors.[5, 11, 12] For example, a "four-leaf clover" pattern in the synchronous spectrum can indicate either two overlapping peaks whose intensities vary in opposite directions or a peak that steadily shifts in position. The explanation for the pattern can be discerned by evaluating the asynchronous spectrum. A four-leaf clover can be assigned to overlapping peaks exhibiting opposite changes in intensity if the asynchronous pattern contains either no peaks (if changes are simultaneous) or one pair of complimentary peaks (above and below the diagonal if the intensity changes are temporally separated). On the other hand, a four-leaf clover in the synchronous spectrum can be assigned to a peak shifting in position if the asynchronous spectrum contains a distinct "butterfly" pattern. The importance of such patterns is apparent in Chapter 4.

Two-dimensional correlation analysis has gathered momentum due to the numerous advantages it provides. It allows for the simplification of complex spectra containing overlapped peaks. Additionally, one obtains enhancement in spectral resolution due to the spreading of data over a second dimension. It is possible to establish unambiguous assignments through correlation of bands, as well as determine specific sequential order of intensity changes. Furthermore, Noda's efforts have resulted in nearly universal applicability of the technique, which is now regularly applied across different disciplines to examine 'spectral' responses to a variety of perturbation types. While the application of 2D correlation spectroscopy is still predominantly to optical spectra, approximately 1 in 6 published experiments have used other analytical probes,[6] including x-rays, as is the case in Chapters 3 through 5. Although temperature, the most commonly employed perturba-

tion, is used in the following chapters, composition, chemical reactions, and physical processes can also be employed.[6]

Furthermore, the abundant application of 2D correlation spectroscopy has allowed for its further evolution. A summary of this was formulated by Noda in 2008;[6] developments of note are moving window and hetero-correlation analyses. Moving window 2D correlation analysis (MW2D) is designed to probe complicated spectral responses by analyzing smaller subsets of data that are shifted incrementally along the perturbation axis to cover the full set. This analysis allows one to gauge the spectral response at specific points along the perturbation variable rather than the overall response to the full range. Further detail and an example of this technique are presented in Chapter 4. Hetero-correlation analysis is applied to two independent measurements of perturbation-induced dynamic spectra. Most frequently, hetero-spectral correlation is applied to a sample's response to a perturbation probed by two different spectral probes. An example of SAXS-WAXS hetero-spectral correlation analysis is presented in Chapter 4.

1.2   EXPLOSIVES DETECTION

Improvised Explosive Devices (IEDs) continue to be the most effective weapon employed against coalition forces in Iraq and Afghanistan. The Joint Improvised Explosive Device Defeat Organization (JIEDDO) is currently implementing over 300 initiatives to tackle this problem.[14] In this era of persistent conflict and global terrorism, the ability to detect explosives in both war zones and high-security installations can save human lives.

The vast challenge in the detection of explosives is in part due to their nature (e.g., small quantities and low vapor pressure) and in part due to concealment in the field and

interference from contaminants. Common explosives are known to have very low vapor pressures,[15, 16] making vapor-based detection, such as infrared spectroscopy, particularly challenging. Furthermore, military grade explosives are often found in solid solutions, such as RDX in plastic composition C4 (C4) explosive, which further limits their vapor pressures.[17] Detection of solid-state explosives is usually based on identifying trace amounts which requires extreme sensitivity. To compound these intrinsic challenges, explosives are often found concealed in a large variety of dynamic environments.

In a laboratory, when they have been separated from any contaminants, explosives can be detected by many reliable techniques, such as mass spectrometry, ion mobility spectrometry, and fluorescence quenching of polymers.[15, 16] However, few of these techniques can be applied at an airport to screen passengers and even fewer still can be implemented in the desert environments of Iraq to detect hidden IEDs.

Furthermore, in the case of IEDs, it is desirable to accomplish detection at a distance, in order to ensure human safety. Standoff detection systems are being developed based on photodissociation laser-induced fluorescence,[18-20] laser-induced breakdown spectroscopy,[21] terahertz time domain spectroscopy,[22] and Raman spectroscopy.[23-29] In most of these cases, the focus is on improvement of hardware. While this approach has resulted in good progress toward effective long standoff detection, further advancement can be achieved through data analysis algorithms, such as spectral pattern recognition and chemometric-based techniques.[15, 30]

Two-dimensional correlation analysis is well suited for detection applications because of its simplification of complex spectra and enhancement of spectral resolution. Additionally, the unstable nature of explosive compounds lends them to respond strongly

to a thermal perturbation, especially when compared to contaminants, such as humic substances. The possibility of using 2D correlation analysis in conjunction with a thermal modulation is examined in Chapter 2.

1.3   SEMI-CRYSTALLINE MATERIALS

More than two-thirds of the annual commercial production of synthetic polymers is comprised of semi-crystalline materials. The many advantages of these materials, such as light weight, flexibility, chemical resistance and toughness, are the reason they are so abundant in today's society, finding applications in the medical market, electronics, construction, textiles and packaging.[31] Specifically, polyethylene (PE) and polypropylene (PP) dominate the semi-crystalline polymer market with demand for PE and PP in North America just below 40 billion pounds and 21 billion pounds, respectively, in 2006.[32] Demand is expected to grow because low cost and expanding versatility make these polymers prime candidates to substitute for less desirable materials. For example, PE can be used to replace steel in automotive fuel tanks and PP can be used to replace aluminum honeycombs as an impact energy absorber.[33]

PP and PE, like other semi-crystalline materials, spontaneously form a nanocomposite structure that confers strength from its crystalline domains and toughness from the non-crystalline material in between. As such, ultimate physical properties of these materials are directly related to their morphology (the distribution of crystalline and non-crystalline regions). The morphology is primarily a function of molecular characteristics (molecular weight, molecular architecture, etc.) and processing conditions (thermal and flow history).

Fabrication processes with PP and PE include injection molding, film blowing, and fiber spinning, and involve non-isothermal conditions, as well as very strong and complex flow fields (shear, elongational, or mixed). Different processing conditions can alter the spatial organization and alignment of the crystallites, affecting properties such as strength, hardness, and surface texture. For example, the elastic modulus of highly-oriented PE fibers is 100 times that of quiescently crystallized PE.[34]
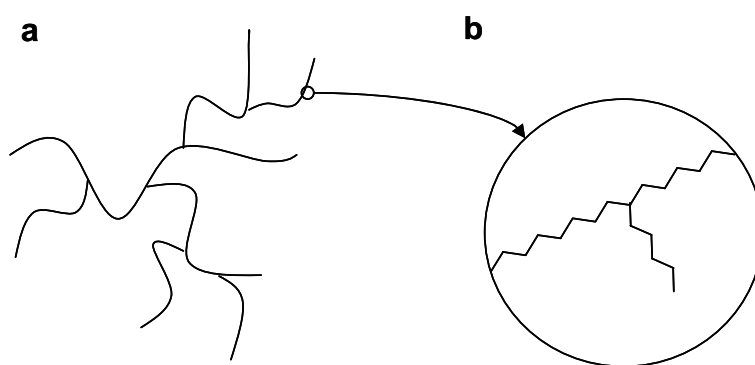
Figure 1.3 Schematic diagram of a polymer containing both long-chain branches evident in **a** and short-chain branches evident in **b**.

In addition, a polymer's molecular characteristics can affect its response to processing conditions. Long-chain branches (LCB) alter melt dynamics affecting the melt's response to a flow field and hence its subsequent morphology. Short-chain branches (SCB) can act as crystal defects decreasing melting temperature and crystallinity.[35] Polymers containing SCB and LCB (Figure 1.3) are of particular interest because of their rich material properties and are examined in Chapter 3. With advances in synthesis, it is now possible to create varying branched polymers on the commercial scale. Low Density PE (LDPE), an LCB and SCB material, and Linear Low Density PE (LLPDE), an SCB material, comprise over half of the current PE market and are used to make films.[36] Therefore, it is of imperative technological relevance to understand the crystallization

process of such linear and branched semi-crystalline materials in order to control their physical properties. Crystallization of SCB materials under flow is examined in Chapter 5. By understanding the behavior of these materials, we can greatly expand the property envelope of semi-crystalline materials, particularly polyolefins.

Polymer crystallization studies employ many probes in order to gain insight into the hierarchy of structures that are formed by semi-crystalline materials. Wide angle x-ray scattering (WAXS) provides insight into the crystal unit cell (i.e., type, dimensions, coherence) that is on the order of angstroms. Small angle x-ray scattering (SAXS) provides insight on the organization of these unit cells into nanoscopic (~10 – 100 nm) structures and distribution of these nanoscopic structures in the non-crystalline regions (e.g., chain-folded lamellar stacks which are on the order of nanometers). Small angle light scattering provides information on the microscopic structure organization, such as spherulites that are on the order of microns. SAXS and WAXS, which are utilized in Chapters 3 through 5, rely heavily upon the analysis of a series of one-dimensional (1D) scattering curves (intensity versus scattering vector). Scattering curves are usually collected as a function of temperature during ramp cooling/heating (crystallization/melting) or time in the case of isothermal crystallization. These experiments result in large datasets with transient behaviors that are well suited for 2D correlation analysis. Its sensitivity to changes in spectral features makes 2D correlation analysis a powerful tool in evaluating morphology development in semi-crystalline systems, as illustrated in Chapter 4 for quiescent crystallization.

1.4   REFERENCES

1. Noda, I., Two-Dimensional Infrared (2D IR) Spectroscopy. *Bulletin of the American Physical Society* **1986,** 31, 520.

2. Noda, I., Two-Dimensional Infrared-Spectroscopy. *Journal of the American Chemical Society* **1989,** 111, (21), 8116-8118.

3. Noda, I., 2-Dimensional Infrared (2d Ir) Spectroscopy - Theory and Applications. *Applied Spectroscopy* **1990,** 44, (4), 550-561.

4. Noda, I., Generalized Two-Dimensional Correlation Method Applicable to Infrared, Raman, and Other Types of Spectroscopy. *Applied Spectroscopy* **1993,** 47, (9), 1329-1336.

5. Noda, I.; Ozaki, Y., *Two-Dimensional Correlation Spectroscopy*. John Wiley & Sons Ltd.: West Sussex 2004.

6. Noda, I. In *Recent advancement in the field of two-dimensional correlation spectroscopy*, 2008; Elsevier Science Bv: 2008; pp 2-26.

7. Noda, I., Determination of Two-Dimensional Correlation Spectra Using the Hilbert Transform. *Applied Spectroscopy* **2000,** 54, (7), 994-999.

8. Jia, Q.; Wang, N. N.; Yu, Z. W., An Insight into Sequential Order in Two-Dimensional Correlation Spectroscopy. *Applied Spectroscopy* **2009,** 63, (3), 344-353.

9. Czarnecki, M. A., Interpretation of two-dimensional correlation spectra: Science or art? *Applied Spectroscopy* **1998,** 52, (12), 1583-1590.

10. Hu, Y.; Li, B. Y.; Sato, H.; Noda, I.; Ozaki, Y., Noise perturbation in functional principal component analysis filtering for two-dimensional correlation spectroscopy: Its

theory and application to infrared spectra of a poly(3-hydroxybutyrate) thin film. *Journal of Physical Chemistry A* **2006,** 110, (39), 11279-11290.

11. McNavage, W.; Dai, H. L., Two-dimensional cross-spectral correlation analysis and its application to time-resolved Fourier transform emission spectra of transient radicals. *Journal of Chemical Physics* **2005,** 123, (18), 12.

12. Gericke, A.; Gadaleta, S. J.; Brauner, J. W.; Mendelsohn, R., Characterization of biological samples by two-dimensional infrared spectroscopy: Simulation of frequency, bandwidth, and intensity changes. *Biospectroscopy* **1996,** 2, (6), 341-351.

13. Morita, S.; Miura, Y. F.; Sugi, M.; Ozaki, Y., New correlation indices invariant to band shifts in generalized two-dimensional correlation infrared spectroscopy. *Chemical Physics Letters* **2005,** 402, (1-3), 251-257.

14. Joint Improvised Explosive Device Defeat Organization. www.jieddo.dod.mil

15. Steinfeld, J. I.; Wormhoudt, J., Explosives detection: A challenge for physical chemistry. *Annual Review of Physical Chemistry* **1998,** 49, 203-232.

16. Moore, D. S., Instrumentation for trace detection of high explosives. *Review of Scientific Instruments* **2004,** 75, (8), 2499-2512.

17. *Proceedings of the First International Symposium on Explosive Detection Technology* U.S. Department of Transportation: Atlantic City, NJ, May 1992, p 988.

18. Arusi-Parpar, T.; Heflinger, D.; Lavi, R., Photodissociation followed by laser-induced fluorescence at atmospheric pressure and 24 degrees C: a unique scheme for remote detection of explosives. *Applied Optics* **2001,** 40, (36), 6677-6681.

19. Wynn, C. M.; Palmacci, S.; Kunz, R. R.; Clow, K.; Rothschild, M. In *Detection of condensed-phase explosives via laser-induced vaporization, photodissociation, and resonant excitation*, 2008; Optical Soc Amer: 2008; pp 5767-5776.

20. Wynn, C. M.; Palmacci, S.; Kunz, R. R.; Rothschild, M., A Novel Method for Remotely Detecting Trace Explosives. *Lincoln Laboratory Journal* **2008,** 17, (2), 27-39.

21. Czarnecki, M. A., Two-dimensional correlation spectroscopy: Effect of normalization of the dynamic spectra. *Applied Spectroscopy* **1999,** 53, (11), 1392-1397.

22. Hua, Z.; Redo, A.; Yunqing, C.; Xi-Cheng, Z., THz wave standoff detection of explosive materials. *Proceedings of the SPIE - The International Society for Optical Engineering* **2006,** 6212, 62120L-1-62120L-62120L-8.

23. Carter, J. C.; Angel, S. M.; Lawrence-Snyder, M.; Scaffidi, J.; Whipple, R. E.; Reynolds, J. G., Standoff Detection of High Explosive Materials at 50 Meters in Ambient Light Conditions Using a Small Raman Instrument. *Applied Spectroscopy* **2005,** 59, (6), 769-775.

24. Carter, J. C.; Scaffidi, J.; Burnett, S.; Vasser, B.; Sharma, S. K.; Angel, S. M., Standoff Raman detection using dispersive and tunable filter based systems. *Spectrochimica Acta Part A* **2005,** 61, 2288-2298.

25. Comanescu, G.; Manka, C. K.; Grun, J.; Nikitin, S.; Zabetakis, D., Identification of explosives with two-dimensional ultraviolet resonance Raman spectroscopy. *Applied Spectroscopy* **2008,** 62, (8), 833-839.

26. Eckenrode, B. A.; Bartick, E. G.; Harvey, S. D.; Vucelick, M. E.; Wright, B. W.; Huff, R. A., Portable Raman Spectroscopy Systems for Field Analysis. *Forensic Science Communications* **2001,** 3, (4).

27. Grasso, R. J.; Russo, L. P.; Barrett, J. L.; Odhner, J. E.; Egbert, P. I., An accurate modeling, simulation, and analysis tool for predicting and estimating Raman LIDAR system performance. *Proceedings of the SPIE - The International Society for Optical Engineering* **2007,** 6681, (1), 66810D-1-66810D-66810D-18.

28. Hayward, I. P.; Kirkbride, T. E.; Batchelder, D. N.; Lacey, R. J., Use of a Fiber Optic Probe for the Detection and Identification of Explosive Materials by Raman-Spectroscopy. *Journal of Forensic Sciences* **1995,** 40, (5), 883-884.

29. Sharma, S. P.; Lahiri, S. C., Absorption spectroscopic and FTIR studies on EDA complexes between TNT (2,4,6-trinitrotoluene) with amines in DMSO and determination of the vertical electron affinity of TNT. *Spectrochimica Acta Part a-Molecular and Biomolecular Spectroscopy* **2008,** 70, (1), 144-153.

30. Brown, S. D.; Barker, T. Q.; Larivee, R. J.; Monfre, S. L.; Wilk, H. R., Chemometrics. *Analytical Chemistry* **1988,** 60, (12), R252-R273.

31. *Modern Plastics World Encyclopedia*. The McGraw-Hill Companies, Inc.: New York, NY, 2000.

32. Plastics News. www.plasticsnews.com

33. *Modern Plastics Encyclopedia*. The McGraw-Hill Companies, Inc: New York, NY, 1999.

34. Ehrenstein, G. W., *Polymeric Materials: Structure, Properties, Applications*. Hanswer Gardner Publications, Inc.: Cincinnati, Ohio, 2001.

35. Bustos, F.; Cassagnau, P.; Fulchiron, R., Effect of molecular architecture on quiescent and shear-induced crystallization of polyethylene. *Journal of Polymer Science Part B - Polymer Physics* **2006,** 44, (11), 1597-1607.

36. Lal, S.; Grady, N. K.; Kundu, J.; Levin, C. S.; Lassiter, J. B.; Halas, N. J., Tailoring plasmonic substrates for surface enhanced spectroscopies. *Chemical Society Reviews* **2008,** 37, 898-911.